Journal of Applied Physics

RESEARCH ARTICLE | NOVEMBER 03 2022

Doped Ru to enable next generation barrier-less interconnect

A. Joi; A. Lesniewska; D. Dictus; ... et. al

Journal of Applied Physics 132, 175704 (2022)
https://doi.org/10.1063/5.0108688

View Online

Export Citation

CrossMark

Articles You May Be Interested In

Advanced concepts for TDDB reliability in conjunction with 3D stress

AIP Conference Proceedings (June 2014)

Physical model for the frequency dependence of time-dependent dielectric breakdown (TDDB)

AIP Advances (May 2023)

Impact of carbon-doping on time dependent dielectric breakdown of SiO_2-based films

Appl. Phys. Lett. (February 2015)

AIP Publishing

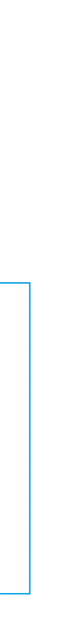
Downloaded from http://pubs.aip.org/aip/jap/article-pdf/doi/10.1063/5.0108688/16519722/175704_1_online.pdf

Journal of Applied Physics | ARTICLE | scitation.org/journal/jap

Doped Ru to enable next generation barrier-less interconnect

Cite as: J. Appl. Phys. **132**, 175704 (2022); doi: 10.1063/5.0108688
Submitted: 9 July 2022 · Accepted: 27 September 2022 ·
Published Online: 3 November 2022

A. Joi,[1] A. Lesniewska,[2] D. Dictus,[1,2,a)] K. C. Tso,[3,4] K. Venkatraman,[1] Y. Dordi,[1,b)] K. Croes,[2] Z. Tokei,[2] S. K. Yadav,[5,6] and P. W. Wu[7,c)]

AFFILIATIONS

[1]Lam Research Corporation, 4650 Cushing Parkway, Fremont, California 94538, USA
[2]IMEC, Kapeldreef 75, Leuven 3001, Belgium
[3]Graduate Program of Accelerator Light Source, National Yang Ming Chiao Tung University, Hsinchu 300, Taiwan
[4]Division of Materials Science, Graduate School of Science and Technology, Nara Institute of Science and Technology, 8916-5 Takayama, Ikoma, Nara 630-0192, Japan
[5]Metallurgical and Materials Engineering, Indian Institute of Technology, Chennai 600036, India
[6]Center for Atomistic Modelling and Materials Design, Indian Institute of Technology, Chennai 600036, India
[7]Department of Materials Science and Engineering, National Yang Ming Chiao Tung University, Hsinchu 300, Taiwan

[a)]**Electronic mail:** dries.dictus@imec.be
[b)]**Electronic mail:** yezdi@dordi.us
[c)]**Author to whom correspondence should be addressed:** ppwu@nycu.edu.tw

ABSTRACT

An effective method for the formation of a Zn-doped Ru liner is demonstrated that realizes a self-forming barrier to achieve low resistivity interconnects for future back-end of line interconnect nodes. The "Ru–Zn" exhibits significantly improved adhesion to the dielectric and better electrochemical nucleation as compared to those of pristine Ru. In addition, time-dependent dielectric breakdown (TDDB) measurements indicate the inhibition of Cu ions drifting into the dielectric that precedes the TDDB failure. Complementary analysis using x-ray absorption spectroscopy, transmission electron microscope, and energy dispersive spectroscope suggests that the "Ru–Zn" forms an interfacial Zn–Si–O compound, and Zn, being more electronegative than Cu, protects the latter from oxidation. Calculation using density function theory also indicates that the Zn–Si–O compound adopts an intercalated structure at the interface of Ru/dielectric in which Zn occupies the interstitial sites within the Si–O lattice. We propose a twofold mechanism for improved TDDB performance: (1) the intercalated Zn atoms effectively block the diffusion of Cu ions through the dielectric and (2) Zn provides the cathodic protection of Cu that prevents the generation of mobile Cu ions that accelerate the TDDB.

Published under an exclusive license by AIP Publishing. https://doi.org/10.1063/5.0108688

I. INTRODUCTION

The miniaturization of nano-electronic devices to keep pace with "Moore's Law" requires the shrinking of Cu interconnects to <10 nm. However, this poses several technological challenges as a major hurdle in extending the dual damascene architecture is the limited space available for the tri-layer structure consisting of barrier, liner, and Cu interconnect.[1] It is because with a smaller interconnect pitch, the thickness of the barrier layer is unable to be further scaled down without significant deterioration in the device reliability. Moreover, in conjunction with a smaller pitch, the electrically resistive barrier layer occupies a relatively larger portion of the interconnect cross section and, thus, contributes to the overall resistance disproportionately. An additional source of resistance in this type of structure is the electron scattering occurring at the barrier-metal (TaN–Cu) interface and Cu grain boundaries.[2] Finally, the increased electromigration (EM) and stress induced voiding (SIV) due to a higher current density passing through these narrow interconnects are serious concerns for premature device failure.[3]

Downloaded from http://pubs.aip.org/aip/jap/article-pdf/doi/10.1063/5.0108688/16519722/175704_1_online.pdf

Published under an exclusive license by AIP Publishing
This article may be downloaded for personal use only. Any other use requires prior permission of the author and AIP Publishing. This article appeared in A. Joi, A. Lesniewska, D. Dictus, K. C. Tso, K. Venkatraman, Y. Dordi, K. Croes, Z. Tokei, S. K. Yadav, P. W. Wu; Doped Ru to enable next generation barrier-less interconnect. Journal of Applied Physics 7 November 2022; 132 (17): 175704. and may be found at https://doi.org/10.1063/5.0108688

One approach that has been explored in the last decade is the so-called self-forming barrier. This has been achieved by doping Cu with impurities such as Mn and Zn.[4–12] Self-forming barriers are interfacial silicates that are formed when the dopants (i.e., Mn and Zn) diffuse across the Cu/liner and reactively segregate at the metal–dielectric interface. The presence of self-forming barrier relaxes the requirement for a thick TaN, thereby reducing the line resistances substantially.[11] However, there are several issues that hinder the implementation of Mn or Zn-based self-forming barrier in a dual damascene process flow. For example, to date the only established method for Cu-Mn deposition is physical vapor deposition (PVD).[6–10] Unfortunately, the PVD is a line-of-sight operation which is not scalable to the sub-10 nm node due to the stringent requirement for deposition conformality. Second, on a per atomic percentage basis, Mn is known to increase the resistivity of Cu substantially.[4,5] On the other hand, the electrochemical atomic layer deposition (e-ALD) has been utilized for Cu–Zn deposition.[11] Although the e-ALD addresses some of the issues relating to Cu–Mn, it introduces additional drawbacks of its own. It is because despite a highly conformal deposit with a lower resistivity than that of Cu-Mn,[13] the e-ALD derived Cu–Zn has a rather limited Zn concentration in the order of ∼1 at. %.[11]

One alternative approach that is more integration-friendly is to introduce the dopant during the liner deposition through a doped liner. Since the liner deposition is intrinsically conformal owing to the layer-by-layer nature of ALD, this resolves the poor conformality associated with the PVD-derived Cu-Mn. Second, the composition for liner material could be tuned readily by optimizing relevant processing parameters and introducing appropriate dopant precursors during ALD cycles. In the literature, the ALD of secondary and ternary compounds is well known.[14,15] For example, Motoyama *et al.* studied the Co-doped Ru liner and reported an improved electron migration (EM) resistance because the Co-doped Ru liner was able to retard the diffusion of Co that was present at the top of the interconnect into the Ru liner.[16] However, this scheme still requires a TaN barrier because Co is not able to form a self-forming barrier. As stated earlier, Zn is a better doping element than Mn. Therefore, we rationalized that the Zn-doped Ru liner might exhibit impressive self-forming barrier characteristic for Cu interconnects smaller than 10 nm.

In this work, we demonstrated a process for preparing a Zn-doped Ru liner and validated its impressive performance as a barrier layer used in the Back End of Line (BEOL) metallization. We also discuss barrier formation mechanisms based on physical, chemical, and electrical characterizations.

II. SAMPLE PREPARATION AND EXPERIMENTAL SETUP

A. Preparation of Zn-doped Ru liner

The doping of Ru with Zn was achieved via a chemical vapor deposition (CVD). Thermal reduction of diethyl zinc (DEZ) with H_2 is a well-known process and a similar process without further modification was adopted for the current study.[17,18] In short, a vacuum chamber equipped with a rough pump and temperature-controlled pedestal was utilized for doping of Ru. The pedestal temperature was set at 350 °C, and the operating pressure was ∼4.5 Torr. H_2 and Ar were used as the carrier gas. The DEZ was introduced into the chamber through a vapor draw precursor delivery system controlled by a manual valve, and its dosage was determined by the duration for which the valve was kept open during the doping process. In our case, the doping time was between 300 and 600 s. Following the doping of DEZ, Ru was annealed at 350 °C in a H_2 ambient for 10 min to render the segregation of Zn. The DEZ was of 99.99% purity and was purchased from Sigma-Aldrich. The Ru test structures (blankets and otherwise) were provided by IMEC. Cu and Cu-Zn (1 at. % Zn) were deposited by PVD using a pristine Cu or CuZn target.

B. Planar capacitors (PCAPs) test vehicle for barrier characterization

To investigate the metal drift barrier properties of Ru–Zn, two sets of PCAPs[19] were used. The first sample, as shown in Fig. 1(a), was a stack consisted of 40 nm Plasma Enhanced Chemical Vapor

Downloaded from http://pubs.aip.org/aip/jap/article-pdf/doi/10.1063/5.0108688/16519722/175704_1_online.pdf

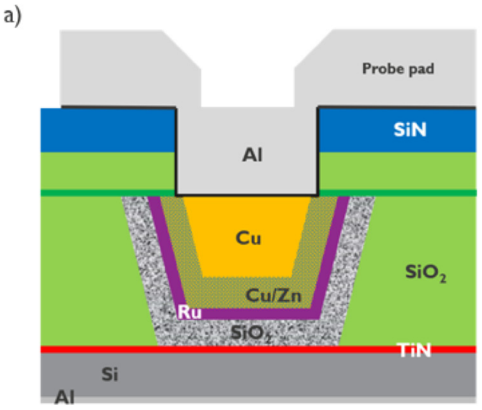

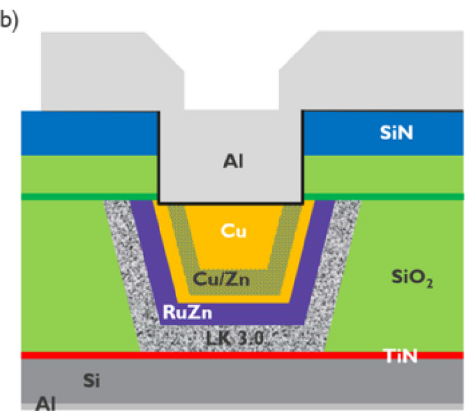

FIG. 1. The schematic of PCAP structures used for metal drift study; (a) sample 1 serving as the control sample and (b) sample 2 serving as the sample under study. For both samples, 10 nm PVD TiN is used as the bottom electrode and electrical connection is established via the backside Al.

Published under an exclusive license by AIP Publishing

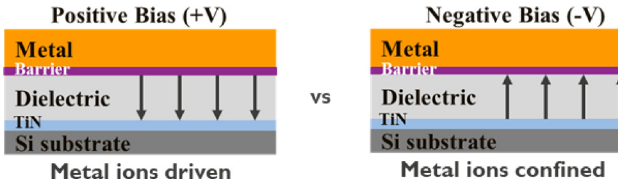

FIG. 2. The schematic of a PCAP under positive and negative stress, respectively.

Deposition (PECVD) SiO_2, 5 nm CVD Ru, 200 nm PVD CuZn, and 300 nm PVD Cu. To protect SiO_2 from moisture intake and Cu from oxidation, as well as to establish the electrical connection, full passivation was placed on top of the stack. After encapsulating the stack, the sample was annealed at 350 °C in forming gas (2:3 N_2/H_2) at 8 Torr for 30 min. The first sample (without Zn in Ru liner) was used as the control sample to compare the performance of RuZn self-forming liner/barrier film as SiO_2, with a dielectric constant of 3.6, is less susceptible to dielectric breakdown and, therefore, would present the "best case scenario." The PCAP structure from the second set (with Zn in Ru liner), as shown in Fig. 1(b), was a stack consisted of 37 nm low-k dielectric[20] (dielectric constant ~3.0) and 5 nm (CVD) RuZn. The sample was annealed for 30 min at 350 °C in forming gas following the doping of Zn so the latter was able to diffuse toward the dielectric–Ru interface. After annealing, the stack was further deposited with 200 nm PVD CuZn, 300 nm PVD Cu, and full passivation, followed by a postannealing at 420 °C in forming gas for 20 min.

The methodology used to determine the metal drift is based on the comparison of field acceleration factor between the positive (metal ions driven) and negative (metal ions confined) stress TDDB. The schematic is depicted in Fig. 2. As the sample was stressed with a negative voltage imposed on the top electrode, the metal ions were unable to enter the dielectric and, thus, the TDDB was caused by the intrinsic dielectric breakdown. On the other hand, as a positive voltage was imposed on the top electrode, the metal ions were driven toward the dielectric once the adhesion layer lacked the necessary metal drift barrier properties. In this case, the TDDB was indicative of metal ions diffusion into the dielectric. The TDDB results from both experiments were fitted using a power-law model (time-to-fail (TTF) ~ electrical field $(E)^{-m}$) because this model allows comparing acceleration factors independent of any small error in thickness/space.[21] It is noted that if the positive and negative field acceleration factors (m) become identical, a negligible metal drift is expected to be detected. In addition, if the slope of TTF vs E for +V stress is smaller than that of −V stress, the metal drift into the dielectric is expected. More details regarding the PCAP methodology could be found in Zhao *et al.*[19]

C. X-ray absorption spectra (XAS)

The x-ray absorption spectroscopy (XAS) for Cu K-edge (8979 eV) and Zn K-edge (9659 eV) was employed to determine the oxidation state and local structure of Cu and Zn in sample 3 and sample 4 (sample 3: SiO_2/Ru/CuZn/Cu; sample 4: SiO_2/RuZn/CuZn/Cu). Note that there existed minor differences between the structures used for PCAP and XAS analysis. For example, the SiO_2 thickness for XAS samples was 200 nm. In addition, samples used in the PCAP test employed a low-k dielectric film which more closely resembles the existing dielectric films used in BEOL for sub-10 nm nodes. However, these minor differences were not expected to impact our observations and conclusions. The XAS measurements were conducted at the BL07A beamline in National Synchrotron Radiation Research Center (NSRRC) in Hsinchu, Taiwan. The photon energy was calibrated using the standard Zn and Cu foils. Analysis from x-ray absorption near-edge structure (XANES) and extended x-ray absorption fine structure (EXAFS) was performed by normalizing the K-edge absorption curves with the removal of background signal by Athena software (IFEFFIT 1.2.12) and IFEFFIT 1.2.11 Artemis software was used for fitting EXAFS spectra. Table I lists the detailed sample specifications in this study and their experimental purpose.

III. RESULTS AND DISCUSSION

A. Characterization of Zn-doped Ru on blanket substrate

There are several criteria that a doped liner should satisfy in order to be considered in a barrier-less BEOL process flow. This has been a heavily explored space in the past decade within the context of Cu–Mn self-forming barrier. These criteria are (1) dopant segregation to the oxygen-rich interfaces, (2) sufficient adhesion to the dielectric to withstand chemical mechanical polishing, (3) dopant out-diffusion maintains the original liner resistivity or incurs a negligible penalty, and (4) dopant provides the protection against liner oxidation and facilitates subsequent Cu electrodeposition. Figure 3 displays the image from transmission electron microscope (TEM) and compositional profiling from the energy dispersive spectroscopy (EDS) showing the self-segregation of Zn toward the O-rich interfaces within a Ru/SiO_2 stack, similar to what would be expected in a dual damascene structure. The sample

Downloaded from http://pubs.aip.org/aip/jap/article-pdf/doi/10.1063/5.0108688/16519722/175704_1_online.pdf

TABLE I. The detailed structural information for our samples and their experimental purpose.

Sample	Insulator	First layer	Second layer	Third layer	Purpose
1	SiO_2 (40 nm)	Ru (5 nm)	Cu-Zn (200 nm)	Cu (300 nm)	PCAP/barrier
2	Low-k 3.0 (37 nm)	Ru–Zn (5 nm)	Cu (10 nm)/Cu–Zn (200 nm)	Cu (300 nm)	PCAP/barrier
3	SiO_2 (200 nm)	Ru (5 nm)	Cu–Zn (200 nm)	Cu (300 nm)	XAS
4	SiO_2 (200 nm)	Ru–Zn (5 nm)	Cu–Zn(200 nm)	Cu (300 nm)	XAS

Published under an exclusive license by AIP Publishing

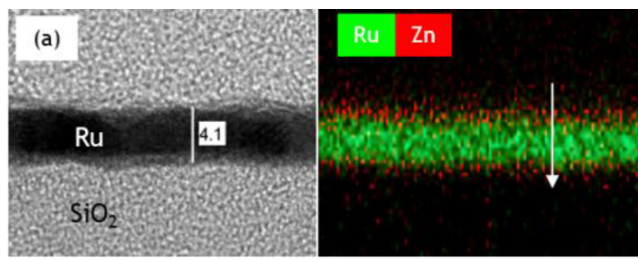

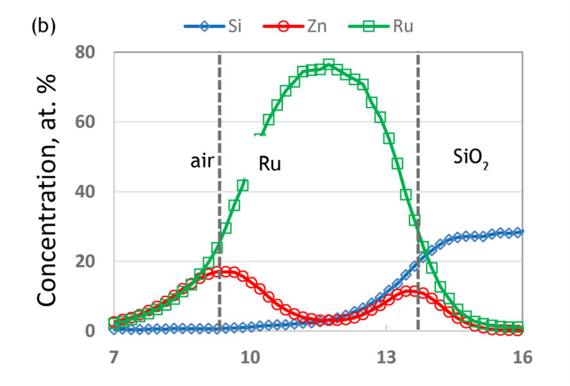

FIG. 3. (a) The cross-sectional TEM image and EDS profile of 4 nm Ru film doped with Zn, followed by 350 °C/10 min annealing in forming gas to drive Zn to the SiO_2 interface. The total dose is equivalent to 600 s of DEZ exposure. (b) The elemental mapping across the Ru/SiO_2 interface showing an accumulation of Zn at the oxygen-rich interface.

was a 4 nm Ru film that was doped with Zn, and followed by an annealing at 350 °C for 10 min in forming gas and subsequently exposed to air. Analysis from EDS indicated the accumulation of Zn at both Ru/SiO_2 and Ru/air interfaces. This is anticipated from the free energy of formation for respective metal oxides as the formation of ZnO is preferred over that of Ru oxides.[22] Moreover, the diffusivity of Zn in Cu and Ru is almost an order of magnitude greater than the self-diffusivity of Ru or Cu,[23] a phenomenon that is responsible for the preferential segregation of Zn. Furthermore, the presence of any Ru–Zn intermetallic is unlikely within the temperature range applicable for BEOL metallization (typically <400 °C). All these factors suggest that the Ru–Zn system could be an ideal candidate for the realization of "barrier-less" interconnect. It is also noted that from Fig. 3(b), the residual Zn concentration in Ru was ∼2 at. %. From our experiences, a longer CVD process targeting a larger Zn doping in Ru rendered the deposition of ZnO on top of Ru. Therefore, we were not able to carry out any further study correlating the amount of Zn doping in the Ru film with the barrier performance.

The second criterion that the Ru–Zn system has to satisfy is robust adhesion to the dielectric. Previously, we had shown enhanced adhesion of e-ALD CuZn/Ru system by a simple scratch tape test.[11] This was attributed to the formation of Zn interfacial compounds. Recently, a more quantitative four-point bending study was carried out by Peng *et al.*[24] They reported that a Zn-doped Ru on the SiO_2 revealed an adhesion energy of 43 J/m^2, a value that was more than ten times greater than that of pure Ru on SiO_2. In addition, analysis from x-ray photoelectron spectroscopy (XPS) on the delaminated interface clearly showed the signals of Zn, which indicated that the formation of interfacial Zn compound was likely to be responsible for the enhanced adhesion.[24] It is noted that in general, an adhesion energy of ∼4 J/m^2 is necessary between the dielectric and metal for BEOL process flow.

The third criterion is the suitability of Ru–Zn liner for Cu electroplating. A typical concern in the BEOL metallization is that the liner material is susceptible to surface oxidation. This leads to additional pre-treatments to reduce undesirable surface oxides prior to the electroplating step. As a result, queue time management becomes essential for BEOL process flow. We rationalized that with Zn-doped Ru, the segregated Zn would form a passivating ZnO film on Ru protecting the latter from oxidation. This ZnO layer would then be dissolved *in situ* in the acidic Cu plating bath

Downloaded from http://pubs.aip.org/aip/jap/article-pdf/doi/10.1063/5.0108688/16519722/175704_1_online.pdf

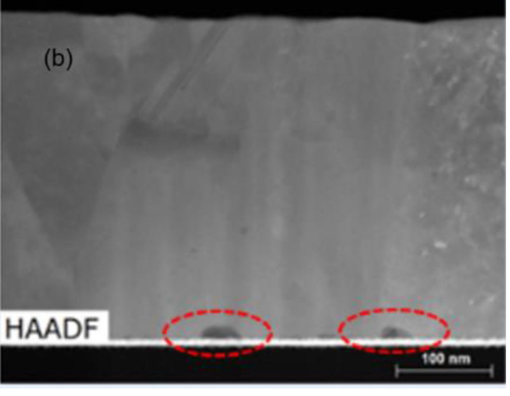

FIG. 4. Cross-sectional STEM images of 450 nm Cu electroplated on (a) Zn-doped Ru and (b) pristine Ru. Both wafers experience ∼3 weeks of air exposure prior to electroplating and no pre-treatment prior to electroplating is applied. A standard acid Cu plating process is used to electroplate Cu.

Published under an exclusive license by AIP Publishing

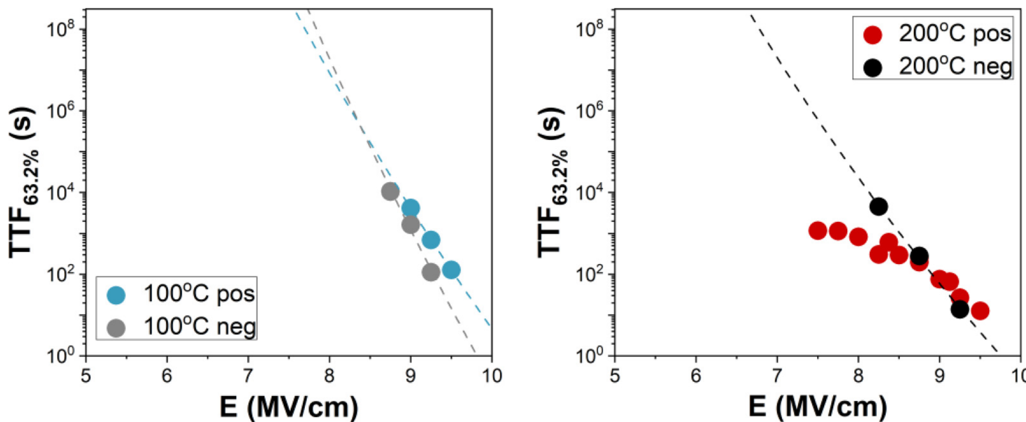

FIG. 5. The TDDB results at 100 and 200 °C for sample 1 (Ru/CuZn/Cu). At both temperatures, the phenomenon of metal drift is evident.

Downloaded from http://pubs.aip.org/aip/jap/article-pdf/doi/10.1063/5.0108688/16519722/175704_1_online.pdf

and electrochemical Cu nucleation would proceed successfully on a pristine Ru surface. Therefore, we expect to have better nucleation and resistivity of Cu plated on Ru–Zn than pristine Ru. This is precisely what is shown in Fig. 4 in which 450 nm Cu was plated on the Zn-doped Ru and pristine Ru without any pre-treatment. The Cu nucleation on the Zn-doped Ru was significantly more robust than that on pristine Ru without pre-treatment. This is evidenced by the lack of any interfacial defects between Cu and Ru in the case of Zn-doped Ru [Fig. 4(a)]. In contrast, there appeared voids at the interface of Cu and Ru for pristine Ru samples [Fig. 4(b)]. In addition, we observed improved thickness and resistivity uniformity on a 300 mm wafer as evidenced by a >4 times reduction in three-sigma parameter (data not included in the paper).

It is noted that a detailed study concerning the resistivity increase in Ru due to the Zn doping was not carried out yet. Although we did not observe any increase in sheet resistance in Ru following Zn doping by simple four-point probe measurements, a more thorough study is warranted and will be reported in a future publication.

B. Characterization of barrier property using PCAP test structure

The TDDB tests were performed on samples at 100 and 200 °C, respectively. The results for sample 1 (Ru/CuZn/Cu stack) are displayed in Fig. 5. Apparently, the results at 100 °C exhibited a smaller field acceleration factor for +V TDDB as compared with that of −V TDDB ($m_{V+} = 64.6 \pm 0.7$ and $m_{V-} = 81.9 \pm 9.1$). This suggested that the metal drift was present during the positive voltage stress. In addition, the tests at 200 °C demonstrated a lack of power-law dependency of TTF vs the E-field for +V TDDB curve. Such behavior was also associated with the metal drift.[19–21,25]

It is expected that CuZn without a Zn-doped Ru liner does not lead to the formation of a self-forming interfacial layer at the dielectric interface that sufficiently prevents the diffusion of Cu through Ru or protects Cu from oxidation, leading to an undesirable drift of Cu^+ ions. On the other hand, sample 2 (RuZn/CuZn/Cu stack) demonstrated improved TDDB results. As displayed in Fig. 6, the overlap of +V and −V at both 100 and 200 °C was observed, which validated a negligible metal ion drift.

Additional results exhibited uniform TTF during TDDB at all temperature/voltage conditions with a Weibull shape parameter of ∼5 (Fig. 7). Such uniform monomodal distributions with a high Weibull shape parameter, which is independent of polarity, stress voltage, and stress temperature suggested the same failure mechanism for all tested samples and further excluded the Cu drift as potential failure mechanism when a positive voltage was imposed.

The cross-sectional EDS analysis of sample 2 (PCAP structure), as shown in Fig. 8, was performed to elucidate the composition at the metal/dielectric interface that was responsible for the improved TDDB and TTF. The EDS analysis on the interface clearly revealed the presence of a finite Zn layer at the interface between Ru and dielectric which likely provided the necessary adhesion for PVD Ru and retarded the Cu ions from drifting into the dielectric during stress. However, further studies are needed to understand the mechanism through which the Zn-doped Ru enhances the adhesion and improves the reliability. It is noted that we also measured the capacitance for our samples and for both SiO_2 and low-k dielectric, the use of CuZn rendered a slightly larger dielectric constant due to the formation of interfacial Zn silicate layer.

C. Characterization of Zn–Si–O complex by XAS

Figure 9 displays the Cu K-edge XANES spectra of sample 3 and sample 4, as well as the standard materials of Cu, Cu_2O, and CuO. In the K-edge XANES profile, the onset photon energy is proportional to the valence state of the absorbing atom, and its magnitude is associated with the electron transition from the 1s to the 4p orbital. Therefore, the valence state of the absorbing atom could be determined by the chemical shifts in the XANES profiles. As shown in Figs. 9(a) and 9(b), the XANES profile for sample 3 was rather close to that of standard Cu_2O. This suggested the presence of Cu^+ in sample 3. It is noted that the XANES profile for sample 4 was identical to that of standard Cu, suggesting that Cu

Published under an exclusive license by AIP Publishing

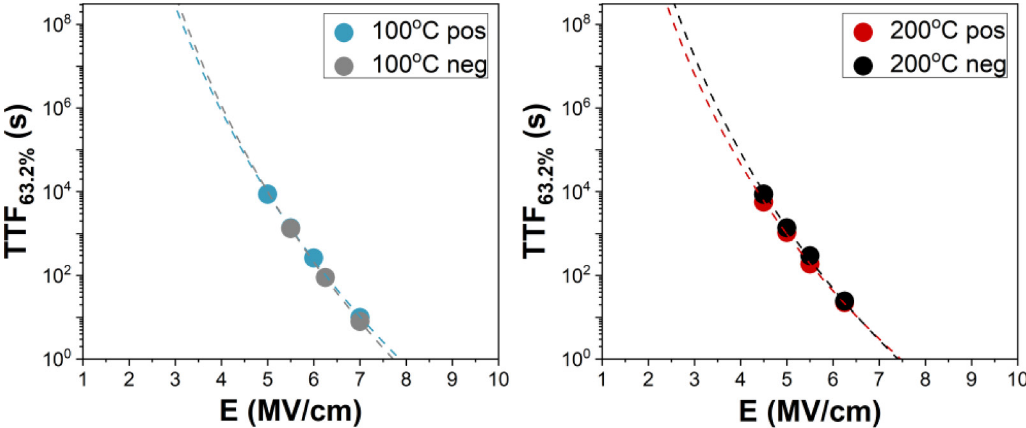

FIG. 6. The TDDB results at 100 and 200 °C for sample 2 (RuZn/CuZn/Cu). At both temperatures, the phenomenon of metal drift is not observed.

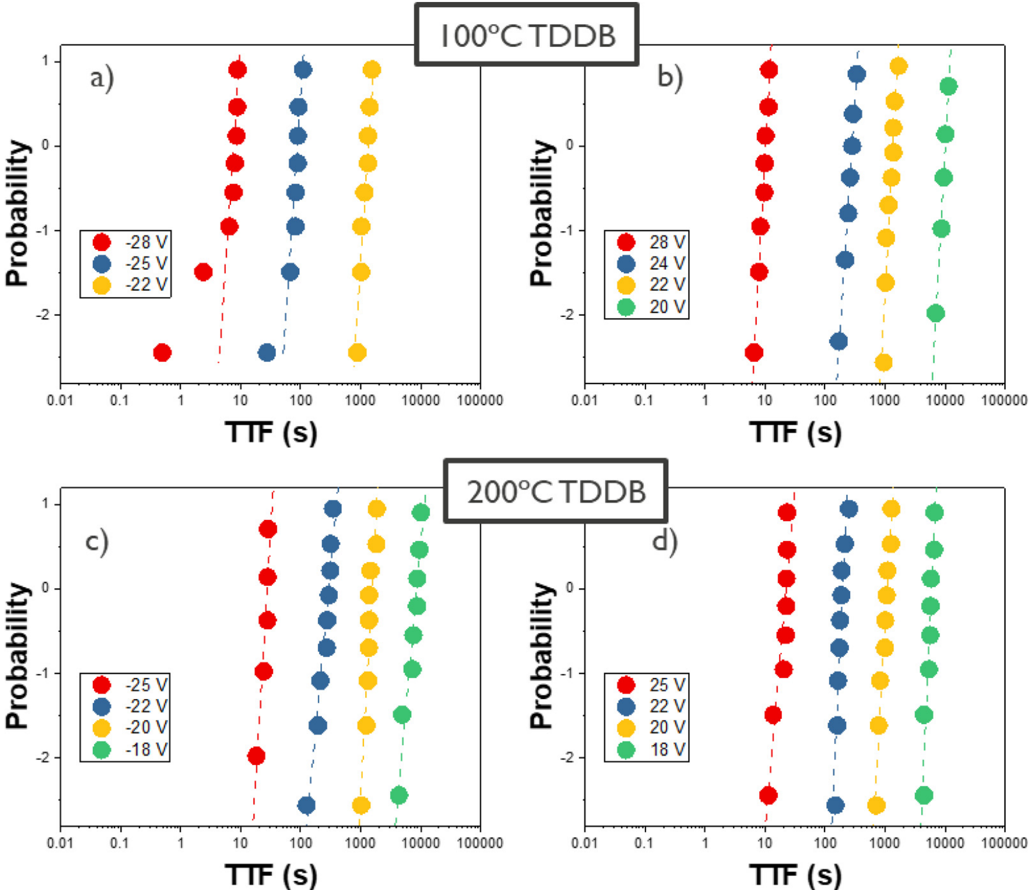

FIG. 7. The Weibull distribution of TTF for sample 2 TDDB data; (a) 100 °C −V TDDB, (b) 100 °C + V TDDB, (c) 200 °C −V TDDB, and (d) 200 °C + V TDDB. All TTF distributions show impressive uniformity.

Downloaded from http://pubs.aip.org/aip/jap/article-pdf/doi/10.1063/5.0108688/16519722/175704_1_online.pdf

Published under an exclusive license by AIP Publishing

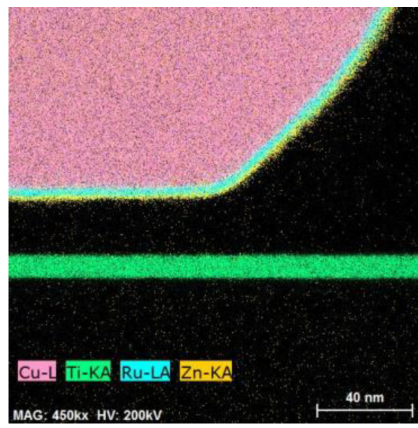

FIG. 8. The cross-sectional EDS analysis for the corner of a PCAP structure showing the diffusion of Zn (yellow) through Ru to produce an adhesion/interfacial layer at the interface between PVD Ru and dielectric.

in sample 4 maintained a metallic state. It is noted that these results were consistent with what we observed in the TDDB experiments in which the Cu ions drift was observed only in sample 1 for which the Zn-doped Ru liner was not present, resulting in the diffusion of Cu to the dielectric interface to become Cu^+. In contrast, sample 2, with a Zn-doped Ru liner, formed a self-forming interfacial layer at the dielectric interface that effectively inhibited the diffusion of Cu to the dielectric interface. Consequently, Cu in sample 4 [Fig. 9(b)] maintained a metallic state. In Fig. 9(c), the Zn K-edge XANES profile for sample 4 was noticeably shifted to that of standard ZnO, suggesting that the valence state of Zn in sample 4 was +2. In addition, the XANES oscillation could be considered a fingerprint for localized structure, and we found that the localized structure for sample 4 was not identical to that of standard ZnO. To further elucidate the microstructure for Zn self-forming interfacial layer at the dielectric interface, the EXAFS fitting of Zn K-edge profiles was performed. It is noted that the EXAFS fitting provides detailed information about the nature of bonding and distance, as well as the number of neighboring atoms. From the EXAFS profiles, the Zn–Zn, Zn–O, and Zn–Si bonds were fitted in the Zn self-forming interfacial layer at the dielectric interface. We explored two distinct theoretical structures to fit the EXAFS profile, and they were Zn_2SiO_4 in $I\bar{4}2d$ space group and SiO_2 in $I\bar{4}2d$ space group (Zn occupying the interstitial sites). Figure 9(d) displays the fitting result using Zn_2SiO_4 in $I\bar{4}2d$ space group. Figure 9(e) displays the fitting result using SiO_2 in $I\bar{4}2d$ space group where Zn occupies the interstitial sites. Apparently, both structures were found to reveal a reasonable match to the EXAFS profile so, in principle, either one of them or both were present at the Ru/dielectric interface. Their corresponding EXAFS fitting parameters are listed in Tables II and III, respectively.

Further considerations lead to the conclusion that Zn_2SiO_4 in $I\bar{4}2d$ space group was unlikely to be present at the Ru/dielectric interface. According to the earlier literature, Zn_2SiO_4 synthesized via various chemical routes is stable in $R\bar{3}$ space group.[26–28] However, the EXAFS fitting using the $R\bar{3}$ space group turned out to be rather poor. It is noted that the volume per formula unit of Zn_2SiO_4 (91 Å^3 in $R\bar{3}$) is approximately twice that of SiO_2 (47 Å^3 in $I\bar{4}2d$ space group). Even if one assumes that oxygen is available to convert SiO_2 to Zn_2SiO_4 in the presence of Zn, the volume would be expected to swell to twice the original volume. Consequently, the presence of Zn_2SiO_4 in $R\bar{3}$ space group is deemed impossible. On the other hand, the presence of monoclinic Zn_2SiO_4 in $I\bar{4}2d$ space group is also unlikely as it requires a large rearrangement of Si–O atoms in SiO_2 that is otherwise in the amorphous state. This rearrangement (crystallization) of SiO_2 is rather difficult, especially at low temperatures. Therefore, the only possible structure at the Ru/dielectric interface is SiO_2 in $I\bar{4}2d$ space group where Zn occupies the interstitial sites.

D. First-principles modeling of Zn–Si–O complex

To determine the structure of Zn–Si–O compound and relate it to the improved TDDB performance, we made a few assumptions and verified those via DFT calculations. As Cu diffuses into SiO_2 as Cu^+ ions that lead to breakdown, we assumed that Zn stops diffusion of Cu ions into SiO_2 by preferentially occupying sites that would otherwise be occupied by Cu^+. If the Zn ions bind the site strongly then it would not diffuse further into SiO_2, hence blocking the diffusion path of Cu ions. We calculated the formation energies of Cu and Zn interstitials in neutral, +1, and +2 charge state in $I\bar{4}2d$ SiO_2. We calculated the formation energies of Cu and Zn interstitials in neutral, +1, and +2 charge state in $I\bar{4}2d$ SiO_2 by using the first-principle DFT as implemented in Vienna Ab initio Simulation Package (VASP)[29,30] and the projector-augmented wave (PAW) method.[31] For all cases, spin-polarized calculations were performed. A plane wave cutoff of 500 eV and a k-point mesh of $2 \times 2 \times 2$ were used for achieving converged results within 10^{-4} eV per atom. All the structures were fully relaxed using the conjugate gradient scheme and relaxations were considered converged when force on each atom was smaller than 0.02 eV/Å.

Interstitial formation energy of Cu and Zn in charge state q $M^q_{SiO_2}$ was calculated using the equation below as described by Freysoldt *et al.*:[32]

$$M^q_{\mathrm{SiO_2}} = E_{M-32(\mathrm{SiO_2})} - E_M - E_{32(\mathrm{SiO_2})} + q(\mu + E_{ref} + \Delta V) + E^q_{corr}, \tag{1}$$

where $E_{M-32(\mathrm{SiO_2})}$ and $E_{32(\mathrm{SiO_2})}$ are the total energies of the one Cu or Zn interstitial in 32 (SiO_2) with charge q and the defect free host supercell having $32(SiO_2)$, respectively. Most stable site of Cu or Zn in $I\bar{4}2d$ SiO_2 is wyckoff 4b (0.0, 0.0, 0.5). E_M is the energy of bulk Cu or Zn atoms in $Fm\bar{3}m$ and $P6_3/mmc$space groups, respectively. E_{ref} is a suitable reference energy which is generally taken to be the valence band maximum (VBM), and the energy of the highest occupied level μ corresponds to the electronic chemical potential. ΔV is the correction to realign the reference potential in the defect supercell with that in the defect free supercell. E^q_{corr} is the correction to the electrostatic interaction and the finite size of the supercell. In this work, we have taken only the first-order monopole correction into account. Here, it must be noted that μ is controlled by the Fermi level of metal interfaced with oxide. If the Fermi level aligns

Downloaded from http://pubs.aip.org/aip/jap/article-pdf/doi/10.1063/5.0108688/16519722/175704_1_online.pdf

Published under an exclusive license by AIP Publishing

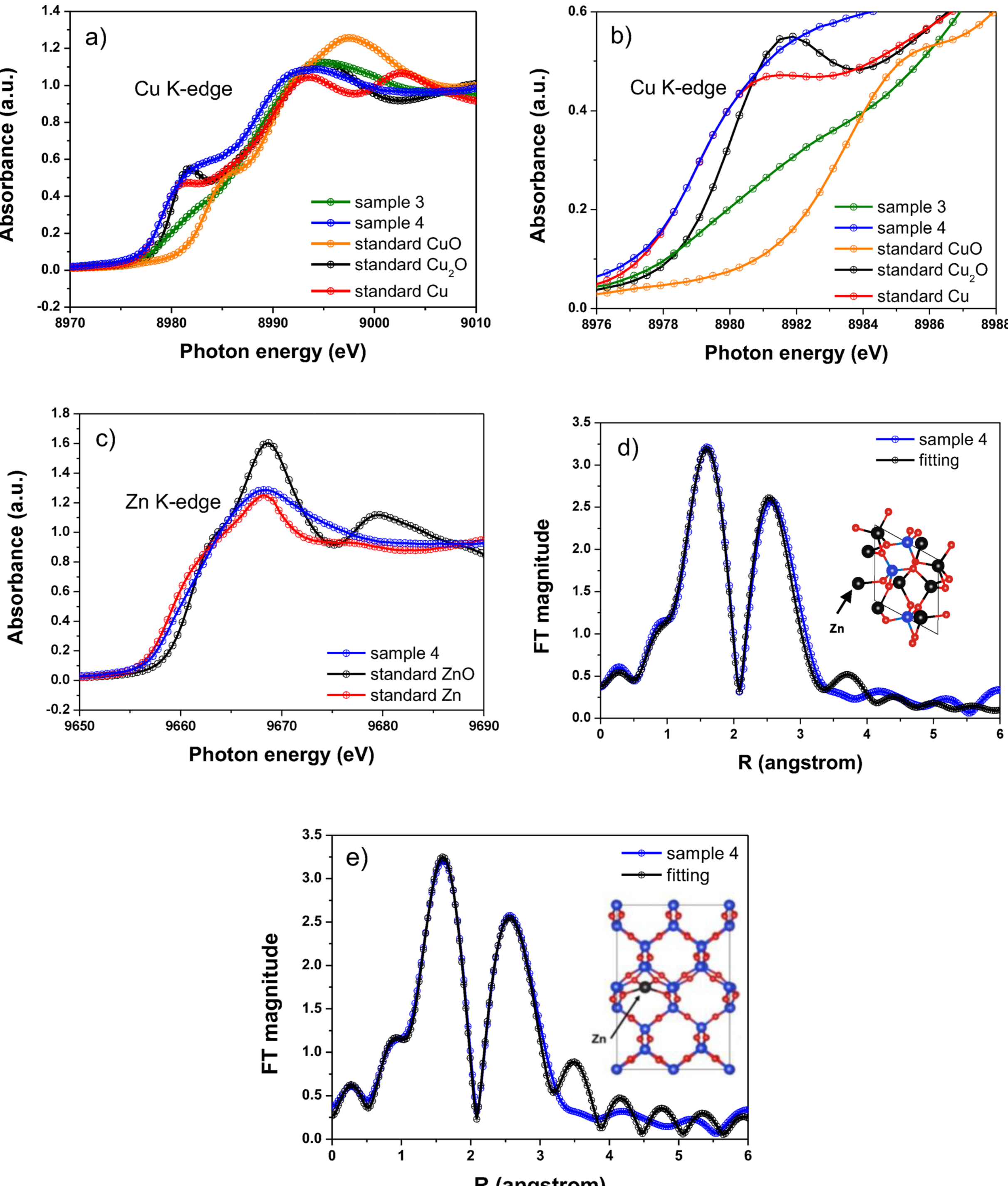

FIG. 9. (a) The Cu K-edge XANES spectra of sample 3 and sample 4, as well as the standard Cu, Cu_2O, and CuO. (b) The zoom-in spectra of (a). (c) The Zn K-edge XANES spectra of sample 4, as well as the standard Zn and ZnO. (d) The k^3-weighted Fourier-transformed-EXAFS profile of sample 4 with the fitting curve associated with Zn_2SiO_4 in $I\bar{4}2d$ space group. (e) The k^3-weighted Fourier-transformed-EXAFS profile of sample 4 with the fitting curve associated with SiO_2 in $I\bar{4}2d$ space group where Zn occupies the interstitial sites.

Downloaded from http://pubs.aip.org/aip/jap/article-pdf/doi/10.1063/5.0108688/16519722/175704_1_online.pdf

Published under an exclusive license by AIP Publishing

TABLE II. The fitting parameters for Zn K-edge EXAFS profile using Zn_2SiO_4 in $I\bar{4}2d$ space group.

Theoretical model	Path	Coordination number	Bond distance, R (Å)	Debye–Waller factor, $\Delta\sigma_j^2$ ($\times 10^{-3}$ Å^2)	R-factor
Zn_2SiO_4	Zn–O_1	1.80	2.05	14.08	0.008
	Zn–O_2	1.80	2.05	14.08	
	Zn–O_3	1.80	3.14	14.08	
	Zn–Si_1	1.80	2.95	4.06	
	Zn–Si_2	1.80	3.07	4.06	
	Zn–Zn_1	3.60	3.45	17.64	
	Zn–Zn_2	1.80	3.59	17.64	

with VBM, μ is zero, if it aligns with CBM, μ is equal to the bandgap of the oxide. μ is equal to the bandgap of the material if it is not interfaced with metal.

Figure 10(a) shows interstitial formation energy of Zn and Cu in various charge states in SiO_2, as a function of electronic chemical potential. Electronic chemical potential refers to the Fermi level of adjoining metal layer; in this case, it is Ru. It suggests that Cu is stable in +1 charge state and Zn is stable in +2 charge state. Interstitial formation energy of Cu^+ is −0.1 eV and that of Zn^{+2} is −2.1 eV, when electronic chemical potential is zero. Formation of interstitial requires that when metal intercalates into an insulator (SiO_2 in this case), the charge released by metal should be accepted by an electronic reservoir (Ru in this case.) Thus, having an oxygen termination is not a pre-requirement for Cu or Zn to diffuse into SiO_2. Figure 10(b) shows the atomic structure of Zn^{+2} and Cu^+ interstitial in SiO_2 ($I\bar{4}2d$ space groups). Zn–O bonds are closer than Cu–O bonds, indicating strong bond between Zn and O compared to Cu and O, in line with interstitial formation energy.

It is noted that SiO_2 in $I\bar{4}2d$ space group is the most stable among various possible structures that SiO_2 could adopt. Modeling in other space groups would not guarantee to be a better representation of amorphous structure. In fact, a good fit between the calculated and the experimental EXAFS spectrum and to Zn_2SiO_4 in $I\bar{4}2d$ space group does not guarantee the presence of the structure. In addition to EXAFS fitting, information like measured stoichiometry should be used to understand the structure. Since our intent is to understand the relative stability of Cu and Zn ions in SiO_2, we rationalize that any stable structure of SiO_2 should serve the purpose.

E. Discussion

Our finding indicated that during annealing, the Zn atoms diffused toward SiO_2 and reacted with SiO_2 occupying available sites at the Ru/SiO_2 interface. At the same time, the Zn atoms were also likely to diffuse upwards to the Cu layer driven by concentration gradient. For desirable barrier and adhesion properties, it is critical for the Zn atoms to fully occupy those available sites at the Ru/SiO_2 interface. This interface could be thought of as 1–2 nm of the dielectric adjacent to Ru in which Zn has reacted with Si–O to form an intercalated structure. To achieve this objective, in the annealing process we employed the forming gas so the majority of Zn atoms (Zn in Cu–Zn and Zn in Ru–Zn) were driven to diffuse toward the Ru/SiO_2 interface. Still, there was a limited diffusion of Zn atoms into the Cu overlayer and the concentration of Zn in Cu did not exceed 1 at. % as this was limited by the availability of Zn atoms. On the other hand, the Zn atom continued diffusing to the Ru/SiO_2 interface because an intercalation reaction was occurring at the Ru/SiO_2 interface that consumed the arriving Zn atoms. We believed that this diffusion of Zn to the Ru/SiO_2 interface was terminated only after all those available sites at the Ru/SiO_2 interface were occupied (or alternatively when all the available Zn atoms were used up). Therefore, the Cu–Zn layer atop the Ru–Zn layer was expected to behave as a source for Zn. It is noted that in our following experiments, we were able to saturate all available sites by doping barely enough Zn atoms into Ru via the CVD process so the Cu–Zn overlayer was no longer necessary. Since the Zn atoms were driven to the Ru/SiO_2 interface due to its favorable thermodynamic consideration, we observed that the Zn atoms were able to diffuse into the Cu overlayer once all the available sites at the Ru/SiO_2 interface were occupied. As a result, we expected that the concentration of Zn atoms in the Cu overlayer to be at the trace level and, thus, its impact on the barrier property became rather negligible.

It is interesting to note that there appeared a lower TTF in the negative direction for Ru–Zn in Fig. 6, as compared to that of Ru in Fig. 5. This is because the experimental substrate in Fig. 6 is an

TABLE III. The fitting parameters for Zn K-edge EXAFS profile using SiO_2 in $I\bar{4}2d$ space group where Zn occupies the interstitial sites.

Theoretical model	Path	Coordination number	Bond distance, R (Å)	Debye–Waller factor, $\Delta\sigma_j^2$ ($\times 10^{-3}$ Å^2)	R-factor
SiO_2 ($I\bar{4}2d$)	Zn–O_1	2.36	2.00	9.75	0.012
	Zn–O_2	2.36	2.75	9.75	
	Zn–Si	1.18	2.97	0.68	
	Zn–O_3	1.18	3.18	9.75	
	Zn–Si_2	1.18	3.39	0.68	

Downloaded from http://pubs.aip.org/aip/jap/article-pdf/doi/10.1063/5.0108688/16519722/175704_1_online.pdf

Published under an exclusive license by AIP Publishing

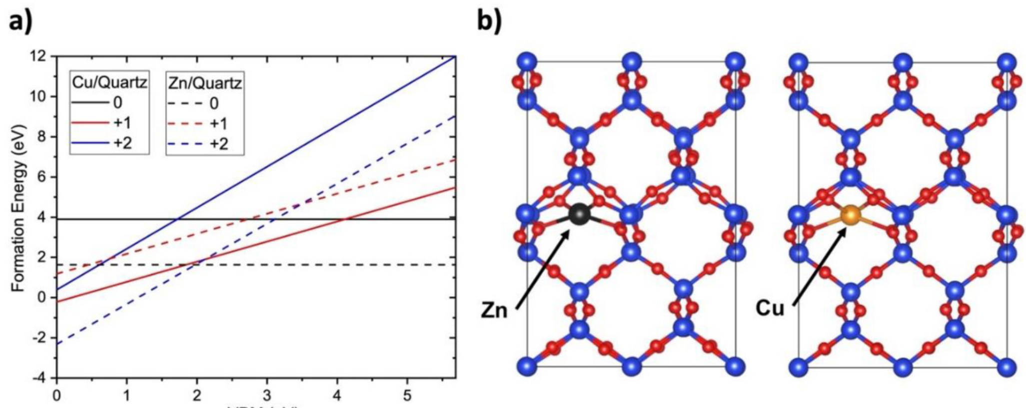

FIG. 10. (a) Interstitial formation energy of Cu and Zn in neutral (0), +1, and +2 as a function of electronic chemical potential. (b) Atomic structure of Zn^{+2} and Cu^{+} interstitial in SiO_2 ($I\bar{4}2d$ space group).

intrinsically weaker (low-k) dielectric. During this part of the test (the negative direction), the failure mode is associated with the dielectric breakdown. It is known that the low-k dielectric is not as strong as SiO_2. However, the low-k dielectric provides significantly better electrical performance (from RC standpoint) and hence it is widely used. Furthermore, the barrier property of the stack is determined by the positive curves. If there is any Cu ion ingress, failure would occur much earlier, which is due to the ion induced leakage current instead of the catastrophic dielectric breakdown. In Fig. 5, at 200 °C the positive curve deviates from the negative slope and exhibits a much lower TTF. At 7.5 MV/cm, the TTF is almost three orders of magnitude lower than that during dielectric breakdown. In the case of Fig. 6, the positive and negative slopes are overlapping, which indicates that negligible metal ion is migrating into the dielectric and dielectric breakdown is the only failure mechanism.

In short, we are proposing that the Zn-doped Ru could serve as a possible replacement for traditional Ta/TaN barrier layer, which is known to be highly resistive. This is supported by our adhesion and TDDB results, which indicate that the Zn-doped Ru is able to limit the diffusion of Cu into the dielectric. Thus, the concept of "barrier-less interconnect" is that the interconnect would be formed without the highly resistive Ta/TaN. This approach would be applicable if the future metallization process employs Ru instead of Cu for interconnects. In addition, the Zn-doped Ru would be a lower resistive alternative for tungsten nitride which is typically used for the adhesion of Ru to dielectric.

IV. CONCLUSION

In this work, we demonstrated an effective process for preparing a Zn-doped Ru liner material and provided reliability characterization that this Ru–Zn could meet the requirements of a barrier layer used in BEOL metallization. The self-forming barrier approach could be a promising candidate for extending the BEOL metallization roadmap to future technology nodes. Exhaustive XAS analysis and DFT calculation shed further light on the chemical nature of the Zn-interfacial layer and the mechanism through which Cu diffusion is retarded. We propose that, in addition to cathodic protection of Cu, Zn also forms an intercalated compound with the dielectric which effectively blocks the diffusion paths for Cu^+.

ACKNOWLEDGMENTS

Professor Satyesh Kumar Yadav and Professor Pu-Wei Wu acknowledge generous donations from Lam Research Corporation and useful discussion with Professor Parasuraman Swaminathan, Professor Lakshman Neelakantan, Mr. Sourva Kanti Maiti, Dr. Debolina Misra, Dr. Soumya Sridar, and Mr. Prince Gollapalli (all from the Indian Institute of Technology), as well as Dr. Jyh-Fu Lee of the National Synchrotron Radiation Research Center.

AUTHOR DECLARATIONS

Conflict of Interest

The authors have no conflicts to disclose.

Author Contributions

A. Joi: Conceptualization (equal); Data curation (lead); Formal analysis (equal); Investigation (equal); Methodology (equal); Writing – original draft (lead); Writing – review & editing (supporting). **A. Lesniewska:** Conceptualization (equal); Data curation (lead); Formal analysis (supporting); Investigation (supporting); Writing – original draft (supporting); Writing – review & editing (supporting). **D. Dictus:** Formal analysis (equal); Investigation (equal); Writing – original draft (supporting); Writing – review & editing (equal). **K. C. Tso:** Formal analysis (supporting); Investigation (supporting); Writing – original draft (supporting); Writing – review & editing (equal). **K. Venkatraman:** Data curation (supporting); Formal analysis (supporting); Investigation (supporting); Writing – original draft (supporting). **Y. Dordi:** Conceptualization (lead); Data curation (supporting); Formal analysis (supporting); Funding acquisition (lead); Resources (equal);

Downloaded from http://pubs.aip.org/aip/jap/article-pdf/doi/10.1063/5.0108688/16519722/175704_1_online.pdf

Published under an exclusive license by AIP Publishing

Supervision (lead); Writing – original draft (lead); Writing – review & editing (supporting). **K. Croes:** Conceptualization (lead); Data curation (supporting); Formal analysis (supporting); Funding acquisition (lead); Investigation (supporting); Resources (equal); Supervision (lead); Writing – original draft (lead); Writing – review & editing (supporting). **Z. Tokei:** Data curation (supporting); Formal analysis (supporting); Investigation (supporting). **S. K. Yadav:** Data curation (supporting); Formal analysis (equal); Methodology (equal). **P. W. Wu:** Formal analysis (equal); Investigation (equal); Methodology (equal); Writing – review & editing (equal).

DATA AVAILABILITY

The data that support the findings of this study are available from the corresponding author upon reasonable request.

REFERENCES

[1] P. C. Andricacos, C. Uzoh, J. O. Dukovic, J. Horkans, and H. Deligianni, "Damascene copper electroplating for chip interconnections," IBM J. Res. Dev. **42**, 567 (1998).
[2] D. Josell, S. H. Brongersma, and Z. Tőkei, "Size-dependent resistivity in nanoscale interconnects," Annu. Rev. Mater. Res. **39**, 231 (2009).
[3] See www.itrs.net for "International Technology Roadmap for Semiconductors."
[4] K. Barmak, C. Cabral, K. P. Rodbell, and J. M. E. Harper, "On the use of alloying elements for Cu interconnect applications," J. Vac. Sci. Technol. B **24**, 2485 (2006).
[5] J. P. Gambino, "Improved reliability of copper interconnects using alloying," in *2010 17th IEEE International Symposium Physics Failure Analysis Integrated Circuits* (IEEE, Piscataway, NJ, 2010), p. 1.
[6] J. Koike and M. Wada, "Self-forming diffusion barrier layer in Cu-Mn alloy metallization," Appl. Phys. Lett. **87**, 041911 (2005).
[7] M. Haneda, J. Iijima, and J. Koike, "Growth behavior of self-formed barrier at Cu-Mn/SiO_2 interface at 250–450(C," Appl. Phys. Lett. **90**, 252107 (2007).
[8] T. Nogami *et al.*, "Electromigration extendibility of Cu(Mn) alloy-seed interconnects, and understanding the fundamentals," in *Technical Digest-International Electron Devices Meeting IEDM* (IEEE, 2012), p. 805.
[9] C. Christiansen *et al.*, "Electromigration-resistance enhancement with CoWP or CuMn for advanced Cu interconnects," in *2011 IEEE International Reliability Physics Symposium 3E.3.1* (IEEE, 2011).
[10] T. K. Indukuri *et al.*, "Electrical and reliability characterization of CuMn self-forming barrier interconnects on low-k CDO dielectrics," Microelectron. Eng. **92**, 49 (2012).
[11] A. Joi *et al.*, "Interface engineering strategy utilizing electrochemical ALD of Cu-Zn for enabling metallization of sub-10 nm semiconductor device nodes," ECS J. Solid State Sci. Technol. **8**, P516 (2019).
[12] T. Nogami *et al.*, "Cobalt/copper composite interconnects for line resistance reduction in both fine and wide lines," in *2017 IEEE International Interconnect Technology Conference (IITC)* (IEEE, 2017), p. 1.
[13] M. César, D. Gall, and H. Guo, "Reducing grain-boundary resistivity of copper nanowires by doping," Phys. Rev. Appl. **5**, 54018 (2016).
[14] K. L. Pickrahn *et al.*, "ALD of ultrathin ternary oxide electrocatalysts for water splitting," ACS Catal. **5**, 1609 (2015).
[15] J. Bakke and K. L. Pickrahn, "Nanoengineering and interfacial engineering of photovoltaics by atomic layer deposition," Nanoscale **3**, 3482 (2011).
[16] K. Motoyama *et al.*, "Co-doped Ru liners for highly reliable Cu interconnects with selective Co cap," in *2020 IEEE International Interconnect Technology Conference (IITC)* (IEEE, 2020), p. 13.
[17] T. Weckman and K. Laasonen, "Atomic layer deposition of zinc oxide: Diethyl zinc reactions and surface saturation from first-principles," J. Phys. Chem. C **120**, 21460 (2016).
[18] J. Cheon *et al.*, "Chemical vapor deposition of zinc from diallyl zinc precursors," Chem. Mater. **6**, 2279 (1994).
[19] L. Zhao, Z. Tikei, G. G. Gischia, H. Volders, and G. Beyer, "A new perspective of barrier material evaluation and process optimization," in *2009 IEEE International Interconnect Technology Conference* (IEEE, 2009), p. 206.
[20] K. Croes *et al.*, "Current understanding of BEOL TDDB lifetime models," ECS J. Solid State Sci. Technol. **4**, N3094 (2015).
[21] K. Croes, P. Roussel, Y. Barbarin, C. Wu, Y. Li, J. Bömmels, and Z. Tőkei, "Low field TDDB of BEOL interconnects using >40 months of data," in *2013 IEEE International Reliability Physics Symposium (IRPS)* (IEEE, 2013), p. 2F-4.
[22] H. J. T. Elingham, "Reducibility of oxides and sulphides in metallurgical processes," J. Soc. Chem. Ind. **63**, 125 (1944).
[23] G. Neumann and C. Tujin, *Self-diffusion and Impurity Diffusion in Pure Metals: Handbook of Experimental Data* (Elsevier Ltd., New York, 2009).
[24] W. Peng, X. P. Qu, and Y. Dordi, "Study of adhesion for Cu/Ru(Zn) on dielectrics by an improved four-point bending measurement," in *2020 IEEE International Interconnect Technology Conference (IITC)* (IEEE, 2020), p. 115.
[25] C. Wu, O. V. Pedreira, A. Leśniewska, Y. Li, I. Ciofi, Z. Tőkei, and K. Croes, "Insights into metal drift induced failure in MOL and BEOL," in *2018 IEEE International Reliability Physics Symposium (IRPS)* (IEEE, 2018), p. 3A-1.
[26] Chakradhar *et al.*, "Solution combustion derived nanocrystalline Zn_2SiO_4: $MnZn_2SiO_4$:Mn phosphors: A spectroscopic view," J. Chem. Phys. **121**, 10250 (2004).
[27] Y. I. Kim, W. B. Im, K. S. Ryu, K. B. Kim, Y. H. Lee, and J. S. Lee, "Combined Rietveld refinement of Zn_2SiO_4:Mn^{2+} using X-ray and neutron powder diffraction data," Nucl. Instrum. Methods Phys. Res., Sect. B **268**, 346 (2010).
[28] S. R. Lukic *et al.*, "Optical and structural properties of Zn_2SiO_4:Mn^{2+} green phosphor nanoparticles obtained by a polymer-assisted sol-gel method," Scr. Mater. **58**, 655 (2008).
[29] G. Kresse and J. Furthmuller, "Efficient iterative schemes for *ab initio* total-energy calculations using a plane-wave basis set," Phys. Rev. B **54**, 11169 (1996).
[30] G. Kresse and J. Furthmuller, "Efficiency of *ab-initio* total energy calculations for metals and semiconductors using a plane-wave basis set," Comput. Mater. Sci. **6**, 15 (1996).
[31] P. E. Blochl, "Projector augmented-wave method," Phys. Rev. B **50**, 17953 (1994).
[32] C. Freysoldt *et al.*, "Electron and chemical reservoir corrections for point-defect formation energies," Phys. Rev. B **93**, 165206 (2016).

Downloaded from http://pubs.aip.org/aip/jap/article-pdf/doi/10.1063/5.0108688/16519722/175704_1_online.pdf

Published under an exclusive license by AIP Publishing